Max-Planck-Institut für Biogeochemie

MPI-BGC Jena

# TECHNICAL REPORTS 18

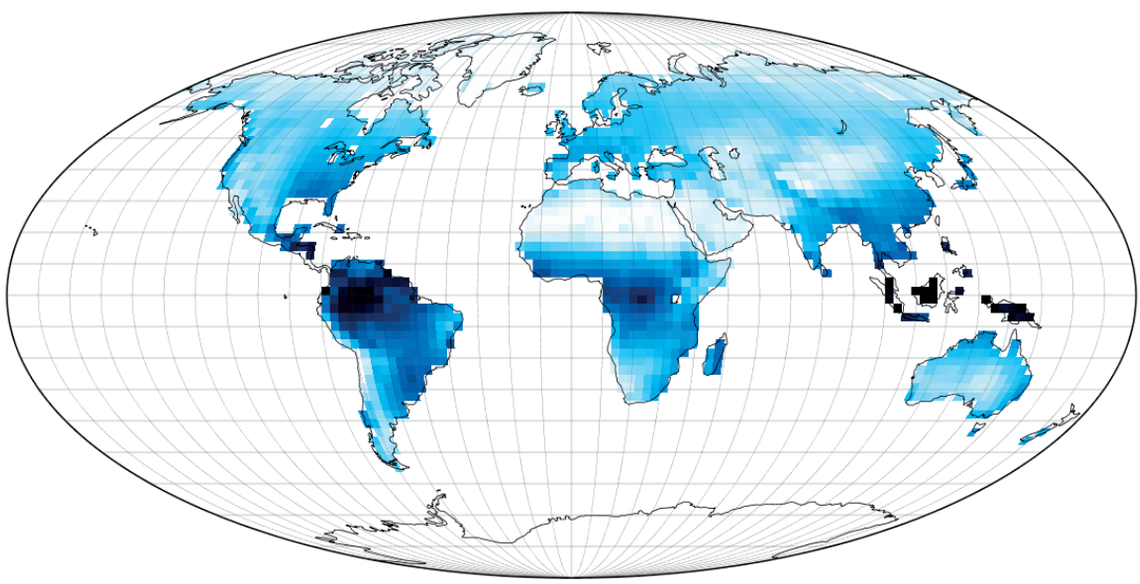

## A simple global land surface model for biogeochemical studies

by
P. Porada, S. Arens, C. Buendia, F. Gans,
S. J. Schymanski and A. Kleidon

ISSN 1615-7400

MAX-PLANCK-GESELLSCHAFT

Technical Reports - Max-Planck-Institut für Biogeochemie 18, 2010

Max-Planck-Institut für Biogeochemie
P.O.Box 10 01 64
07701 Jena/Germany
phone: +49 3641 576-0
fax: + 49 3641 577300
http://www.bgc-jena.mpg.de

# A simple global land surface model for biogeochemical studies

P. Porada*, S. Arens*, C. Buendía*, F. Gans*, S. J. Schymanski* and A. Kleidon *

## Abstract

A simple and global model of terrestrial biogeochemistry is presented here. The model accounts for the most important fluxes of carbon and water at the land surface, such as evapotranspiration, runoff and Net Primary Productivity. Its main feature is modularity, meaning that the different parts of the model can be exchanged. At the moment, for instance, the model consists of a vegetation and a soil model, which are able to run independently and can also be connected to other models. The model is fast and it is able to reproduce a range of observational datasets with good accuracy. It can subsequently be used as a predictive tool in terrestrial biogeochemistry.

## 1. Introduction

The aim of this paper is to present and evaluate a simple and fast model of terrestrial biogeochemistry that runs on a global scale. The model consists of three systems, corresponding to soil, vegetation and atmosphere. In the presented version, the soil system is described by the model JESSY (JEna Soil SYstem model), the vegetation system by the model SIMBA (SIMulator of Biospheric Aspects) and the atmosphere system is represented by a forcing data set. The systems communicate by means of fluxes of matter and energy. Root water uptake, for instance, is written as a flow of water from the soil system to the vegetation system. In this way, carbon, water and heat balances can be quantified.

Due to the compartmentalised model structure, it is easy to replace processes and integrate additional ones into the models. In the current version, for example, JESSY is able to run without SIMBA and can also be connected to a different vegetation model. In turn, SIMBA could be coupled to different kinds of soil models. It is also straightforward to include processes such as weathering or cycling of phosphorus

*Max Planck Institut für Biogeochemie; P.O. Box: 10 01 64, 07701 Jena, Germany

into the model (e.g. (Arens and Kleidon, 2008)).

SIMBA has already been described in Lunkeit et al. (2004), but never been explicitly evaluated. Moreover, the version of SIMBA used in this study has been extensively modified in order to make it compatible with the modular structure of the whole model. Hence, SIMBA is presented here together with JESSY.

In accordance with the modular structure of the framework, the variable names consist of the name of the substance they represent, its phase, and the systems they refer to (see Table 1 and 2). This makes the variable names precise and easy to understand.

At the beginning of this paper, the naming convention for the model and the variables and parameters of the model are described. This is followed by a description of the components of JESSY and SIMBA and an evaluation of the model. The paper closes with a discussion and some brief conclusions.

This article, a user manual and the source code of the model can be found under the following link:

http://www.bgc-jena.mpg.de/service/pr/technical_reports/18/

## 2. Model description

### 2.1. Model structure

Figure 1 gives an overview of the structure of JESSY and SIMBA.

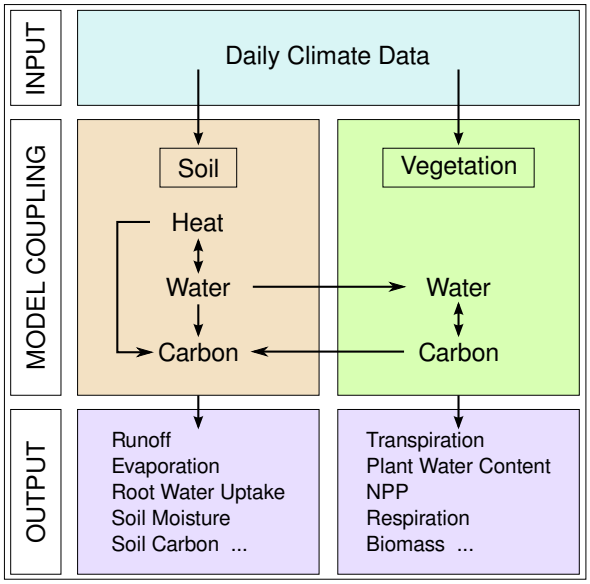


**Figure 1:** Diagram showing the structure of the model, the processing sequence and the most important output variables. JESSY corresponds to the soil part and SIMBA to the vegetation part.

### 2.2. Variable names

In the JESSY and SIMBA models a naming convention for variables has been introduced to secure easy recognition of their meaning. State variables are conventionally named $rA_b^c$ or $xA_b^c$ ($r$ for extensive variables, $x$ for intensive ones) where $A$ is a chemical compound, e.g. $H_2O$, a form of energy, e.g. heat $Q$ or a state variable such as temperature $T$, $b$ is the state of matter, e.g. solid, and $c$ is the location, e.g. atmosphere (see Table 1). Fluxes have names of the form $fA_{bb}^{cc}$, where $bb$ is start and end state (to consider phase change) and $cc$ is the start and end location. Root uptake of water from soil to vegetation is thus named $fH2O_l^{sv}$.

**Table 1:** Abbreviations in variable names

| | | Abbreviation |
|---|---|---|
| State | solid | s |
| | liquid | l |
| | gaseous | g |
| | dissolved | d |
| | structural biomass | o |
| | sugars & starch | c |
| Reservoir | atmosphere | a |
| | vegetation | v |
| | soil | s |
| | river channel | c |

The model parameters are partitioned into effective parameters (*pname*), which are taken from the literature or calibrated, and measurable constants (*cname*). Wherever possible, the parameter names are adapted to the naming convention. The type of parameter is abbreviated by a letter, e.g. $K$ for conductivity or $\tau$ for time scale, and the phase as well as the location are abbreviated as described above. The conductivity for water at the soil-root interface, for instance, is written as $pKH2O_l^{sv}$.

Some important variables and model parameters are listed in Table 2 and Table 3 in the appendix.

## 2.3. Soil Heat

### 2.3.1. General setup

JESSY-HEAT is a heat diffusion scheme that is responsible for calculating heat fluxes into and out of the soil as well as freezing and thawing of soil water. It is the only part of the model that has a vertical structure and uses more than one vertical layer. In the standard version the thickness of the layers is set to 1 m so that only the first layer is coupled to the other model parts. The soil water content, for example affects only the thermal properties of the first layer while all the other layers are modelled with fixed water content.

The module JESSY-HEAT uses a fixed number of soil layers *pnlayer*, each having a thickness equal to the soil depth $p\Delta Z^s$ and being characterised by a dynamic temperature, heat capacity and heat conductivity. In the following equations indices i and j always denote the soil layer, layer 1 being the top layer. The heat flux from layer i to j is calculated by

$$fQ^{s,ij} = \frac{2(xKQ^{s,i} + xKQ^{s,j})(xT^{s,i} - xT^{s,j})}{p\Delta Z^{s,i} + p\Delta Z^{s,j}} \tag{1}$$

The soil conductivities are updated at each time step and depend on the water content of the soil layer (see below). There are two schemes for heat exchange of the soil with the atmosphere, depending on the snow cover. If there is no snow, then the heat flux is only determined by the surface temperature and the soil heat conductivity:

$$fQ^{as} = \frac{2(xKQ^{s,1})(xT^{as} - xT^{s,1})}{p\Delta Z^{s,1}} \tag{2}$$

In the case of surface snow the snow acts as an additional layer. The heat flux between the air and the snow layer is parametrized as:

$$fQ^{as} = pDQ^{as} \cdot (xT^{as} - xT^{s,0}) \tag{3}$$

where $pDQ^{as} = 12.44 W/Km^2$ is a snow/atmosphere boundary heat diffusivity. The value of $pDQ^{as}$ is derived from the PlaSim model (Lunkeit et al., 2004).

The heat exchange between the snow layer and the first soil layer is calculated according to Equation 1. Note that the radiation budget is not considered here.

### 2.3.2. Coupling to soil water

In its standard version the model is run with a layer thickness of 1 m. Thus, only the first layer is affected by soil water. For the heat capacity this means that the heat capacity of the soil water simply adds to the dry soil heat capacity. To include the effect of additional heat conductivity added by the soil water, at each time step the Kersten number is calculated as $Nk = 0.7 \cdot \log_{10}(rH2O_l^s/pmaxH2O_l^s)$ for liquid water (Blackburn et al., 1997). If the temperature is below the melting point, the Kersten number is defined as $Nk = rH2O_l^s/pmaxH2O_l^s$. The soil heat conductivity is then estimated as:

$$xKQ^s = pminKQ^s + (pmaxKQ^s - pminKQ^s) \cdot Nk \quad (4)$$

The water content also has substantial influence on the temperature profile when the melting point is reached. Then the heat added to or removed from the layer is directly transformed into latent heat of fusion. When all the soil water has changed its state, the temperature will change again according to the additional heat flux.

## 2.4. Water balance

Flows of water across the boundary of the soil system and changes in soil water content are described in JESSY-WATER by means of a bucket model. It allows for the quantification of bare soil evaporation, root water uptake, surface runoff and slow baseflow. Water at the land surface is described by means of three state variables: Soil water $rH2O_l^s$, soil ice $rH2O_s^s$, and snow $rH2O_s^{as}$ which have the unit [m]. The state of the soil water is characterised by the degree of saturation, $rH2O_l^s/pmaxH2O_l^s$, where $pmaxH2O_l^s$ is the maximum water storage capacity of the bucket. $pmaxH2O_l^s$ is a product of soil depth $p\Delta Z^s$ and the relative soil water content at saturation $(p\Theta s^s - p\Theta r^s)$ for the soil type sandy loam (see Table 3). Dependent on soil temperature, a certain fraction of the soil water is frozen as soil ice. This water cannot be part of the exchange flows of water and therefore results in a reduced bucket size. The partitioning between soil water and soil ice is calculated in JESSY-HEAT. Snow is stored in a reservoir above the soil.

The input of water into the soil system consists of rainfall $fH2O_l^{as}$ and water from snow-melt $fH2O_{sl}^{as}$. If there is no snow cover on the soil, it is assumed that all rainfall infiltrates into the soil, losses due to infiltration excess flow and evaporation of intercepted rainfall are neglected. If a snow cover exists, however, it is assumed that the soil surface is frozen and all rainfall is converted into surface runoff. Snow melt is calculated in JESSY-HEAT (see Section 2.3) and is added to rainfall. In addition to melting, snow is lost due to the movement of glaciers into the ocean, $fH2O_s^{so}$. This is described by $fH2O_s^{so} = rH2O_s^{as} \cdot p\tau H2O_s^{as}$.

The flows of water out of the soil are quantified as functions of the state of soil water and other variables. Water can leave

the soil in form of surface runoff $fH2O_l^{ac}$, bare soil evaporation $fH2O_g^{sa}$, root water uptake $fH2O_l^{sv}$ and baseflow $fH2O_l^{sc}$. Surface runoff $fH2O_l^{ac}$ is calculated as saturation excess flow:

$$fH2O_l^{ac} = \max\left(0, fH2O_l^{as} + fH2O_{sl}^{as} + \frac{rH2O_l^s + rH2O_s^s - pmaxH2O_l^s}{pdt}\right) \quad (5)$$

where $pdt$ is the time step of JESSY. Bare soil evaporation takes place if soil moisture is high enough. This is assumed to be the case when the expression $pmaxH2O_l^s - rH2O_l^s - rH2O_s^s$ is smaller than 0.01 m. Bare soil evaporation is described as the minimum between available soil water and the potential evaporation under equilibrium conditions (McNaughton and Jarvis, 1983). It is written as:

$$fH2O_g^{sa} = \min\left(\frac{rH2O_l^s + rH2O_s^s + 0.01}{pdt} - \frac{pmaxH2O_l^s}{pdt}, fpotH2O_g^{sa}\right) \quad (6)$$

where

$$fpotH2O_g^{sa} = \frac{\frac{dsdT}{dsdT+c\gamma} \cdot fnet\Gamma}{cQH2O_{lg}} \qquad with$$

$$dsdT = \frac{e^{psa1 \cdot \frac{zT}{psa2+zT}} \cdot psa1 \cdot psa2 \cdot psa3}{(psa2 + zT)^2} \cdot c\rho H2O_l \quad (7)$$

where $dsdT$ is the slope of the saturation vapour pressure versus temperature relationship. $zT$ corresponds to (temperature in K - melting temperature of water, $cTH2O_{sl}$) and $fnet\Gamma$ is net radiation. The values of the parameters $cQH2O_{lg}$, $psa1$, $psa2$, $psa3$, $c\rho H2O_l$ and $c\gamma$ can be found in Table 3). $fH2O_g^{sa}$ is multiplied by the fraction of bare soil in each grid cell since transpiration dominates over evaporation in the presence of vegetation. Note that the phase transition from liquid soil water to water vapour during evaporation ($fH2O_{lg}^{ss}$) is not explicitly modelled here.

Root water uptake depends on the difference in water saturation between the soil and the vegetation:

$$fH2O_l^{sv} = pKH2O_l^{sv}\left(\frac{rH2O_l^s}{pmaxH2O_l^s} - \frac{rH2O_l^v}{pmaxH2O_l^v}\right) \quad (8)$$

where $pKH2O_l^{sv}$ is the conductivity for water flow at the soil-root interface (see Table 3). $\frac{rH2O_l^v}{pmaxH2O_l^v}$ is the relative water content of the vegetation given by SIMBA. The value of $fH2O_l^{sv}$ is transferred to SIMBA where transpiration of water is quantified.

Baseflow is formulated as a function of soil moisture and calculated as:

$$fH2O_l^{sc} = \frac{(rH2O_l^s)^2}{pmaxH2O_l^s \cdot p\tau H2O_l^s} \quad (9)$$

where $p\tau H2O_l^s$ is the time scale of baseflow. The quadratic increase of $fH2O_l^{sc}$ with soil water content accounts for the positive feedback of soil moisture on the hydraulic conductivity of the soil. The flows of water out of the soil are limited to the available water content of the soil. If $fH2O_l^{sv}$ exceeds $rH2O_l^s$, for instance, it is reduced to $rH2O_l^s/pdt$. $fH2O_l^{sc}$ is then set to zero since it is assumed to be a slower process than $fH2O_l^{sv}$.

After the calculation of all flows of wa-

ter, the change in soil water content of the bucket is calculated by the mass balance:

$$\begin{aligned}\frac{d}{dt}rH2O_l^s = {} & fH2O_l^{as} + fH2O_{sl}^{as} \\ & - fH2O_g^{sa} - fH2O_l^{sv} \\ & - fH2O_l^{ac} - fH2O_l^{sc} \\ & - fH2O_{ls}^{ss} + fH2O_{sl}^{ss}\end{aligned} \quad (10)$$

where $fH2O_{ls}^{ss}$ is the amount of water that freezes to soil ice and $fH2O_{sl}^{ss}$ is the amount of melting soil ice, which are both calculated in JESSY-HEAT. The mass balance for the snow reservoir is described by:

$$\frac{d}{dt}rH2O_s^{as} = fH2O_s^{as} - fH2O_{sl}^{as} - fH2O_s^{so} \quad (11)$$

The balance of soil ice is written as:

$$\frac{d}{dt}rH2O_s^s = fH2O_{ls}^{ss} - fH2O_{sl}^{ss} \quad (12)$$

## 2.5. Soil carbon

### 2.5.1. Soil organic carbon

The accumulation and decomposition of soil organic matter $rC_o^s$ is modelled through the influx of litter from SIMBA, $fC_o^{vs}$ (described in Section 2.6, Equation 34) and a Q10 relationship (Knorr and Heimann, 1995):

$$fC_{og}^{ss} = \frac{rC_o^s}{p\tau C_o^s} \cdot pq10ss^{\frac{rT^s - cTH2O_{sl} - 10.0}{10.0}} \quad (13)$$

where $pq10ss$ is the Q10 value, $p\tau C_o^s$ is the residence time of organic matter in the soil and $cTH2O_{sl}$ is the melting temperature of water in K.

### 2.5.2. Soil $CO_2$

The parametrisations of the $CO_2$ balance of the soil are basically the same as in Fang and Moncrieff (1999), but for a box model, i.e. there is only one soil layer. The input of $CO_2$ to the soil comes from three parts: autotrophic/root respiration, litter decomposition/heterotrophic respiration and $CO_2$ dissolved in rain. The loss of $CO_2$ happens through diffusion through the surface, runoff and plant uptake of water. The total amount of $CO_2$ in the soil $rCO2^s$, is

$$rCO2^s = rCO2_g^s + rCO2_d^s = C_g \cdot V_g + C_l \cdot V_l \quad (14)$$

where $C_g$ and $C_l$ are the concentrations of $CO_2$ in the gas and water phases, respectively, and $V_g$ and $V_l$ denote the volumes of those same phases. The combined air and water volume corresponds to the total porosity of the soil, which is constant.

In each time step the total flux of $CO_2$ into the soil from respiration and rain is calculated. However, the variation of the air volume of the soil also plays a role. The air volume in each time step is calculated based on soil wetness. If the air volume is larger than in the time step before, air has diffused in from the atmosphere and thus atmospheric $CO_2$ has been added. If the air volume is less than before, air and thus $CO_2$ has been pushed out of the soil. The water phase contains $CO_2$ that is updated to the current time step using the fluxes of $CO_2$ from the previous time step for rain, plant water uptake and runoff. The new concentrations of $CO_2$ in air and water are assumed to reach equilibrium instantaneously. The equilibrium concentrations are calculated, first for a closed system, i.e. where there is no diffusion out of the system. After this the diffusion to the atmosphere is calculated and finally the

equilibrium calculation is repeated without the diffused $CO_2$. The equilibriums are calculated as follows: The dissolution of $CO_2$ in water under acidic conditions can be described by the following reactions and equilibrium constants:

$$CO_2(g) + H_2O(l) \Leftrightarrow H_2CO_3(aq) \quad (15)$$

$$K_1 = \frac{[H_2CO_3]}{pCO_2} \quad (16)$$

where $pCO_2$ is the partial pressure of $CO_2$ in the soil air (dimensionless) and $K_1$ is the temperature dependent Henry's law constant.

$$H_2CO_3 \Leftrightarrow H^+ + HCO_3^- \quad (17)$$

$$K_2 = \frac{[H^+][HCO_3^-]}{[H_2CO_3]} \quad (18)$$

where $K_2 = 4.1115 \cdot 10^{-7}$ and finally

$$HCO_3^- \Leftrightarrow H^+ + CO_3^{2-} \quad (19)$$

$$K_3 = \frac{[H^+][CO_3^{2-}]}{[HCO_3^-]} \quad (20)$$

$K_2$ and $K_3$ are constants for the ionization reactions of the hydrogen carbonates. The concentration of $CO_2$ in the liquid phase is the sum of the three carbonate species.

$$C_l = [H_2CO_3] + [HCO_3^-] + [CO_3^{2-}] \quad (21)$$

$[CO_3^{2-}]$ can be left out because $[CO_3^{2-}] \ll [HCO_3^-]$ under acidic conditions. Then, this can be rewritten to

$$C_l = \left(K_1 + \frac{K_1K_2}{[H^+]}\right) \cdot pCO_2 \cdot 1000 \quad (22)$$

where $pCO_2$ is the partial pressure of $CO_2$ in the soil air and the factor 1000 is to change $C_l$ from units of $[mol/l]$ to $[mol/m^3]$. $pCO_2$ can be related to $C_g$:

$$pCO_2 = D \cdot C_g \quad (23)$$

where $C_g$ is in units of $[mol/m^3]$ and

$$D = \frac{RT}{pAIR} \quad (24)$$

where $R = 8.314 Jmol^{-1}K^{-1}$ is the molar gas constant and $pAIR$ is the air pressure in Pa. Combining Equations (16) and (18) we get

$$K_1K_2 \cdot pCO_2 = [H^+][HCO_3^-] \quad (25)$$

Since we have left out $[CO_3^{2-}]$, $[H^+] \approx [HCO_3^-]$

$$[H^+] = \sqrt{K_1K_2 \cdot pCO_2} = \sqrt{K_1K_2D \cdot C_g} \quad (26)$$

From Equation (14):

$$C_g = \frac{rCO2^s - C_lV_l}{V_g} \quad (27)$$

substituting (23) and (26) into Equation (22) gives a new expression

$$C_l = \left(K_1 + \frac{K_1K_2}{\sqrt{K_1K_2 \cdot D \cdot C_g}}\right) \cdot D \cdot C_g \cdot 1000 \quad (28)$$

where the factor 1000 changes $C_l$ from units of $[mol/l]$ to $[mol/m^3]$. This can be manipulated into a 2nd order equation for $C_l$ or $C_g$ by applying Equation (27).

## 2.6. Vegetation

The vegetation module is a simplified dynamic parametrisation of terrestrial vegetation accounting for the general water and carbon fluxes through vegetation. Originally, the vegetation module was a part

of the Planet Simulator, PlaSim, (Lunkeit et al., 2004). Now it is presented as a sub-module on its own with considerable changes to the one presented in the PlaSim model documentation. Its main purpose is to predict large-scale vegetation states and fluxes, e.g. the exchange of water and carbon between vegetation, soil and atmosphere. Climate and soil properties set the constraints to vegetation, and vegetation feeds back on the water and carbon fluxes to and from the soil. In the following we will explain how we represent vegetation in terms of the water and carbon fluxes.

### 2.6.1. Carbon fluxes

Net $CO_2$ uptake by photosynthesis, or gross primary productivity (GPP), is calculated as the minimum of $CO_2$-demand and $CO_2$-supply. The demand is driven by the light-dependent reactions of photosynthesis, the supply is limited by the inflow of $CO_2$ into the leaf, which is coupled to the transpiration of water (Monteith et al., 1989; Dewar, 1997; Kleidon, 2004, 2006):

$$fCO2_{gc}^{av} = \min(fCO2_{gc}^{av}[light], fCO2_{gc}^{av}[water]) \tag{29}$$

where the light-driven GPP is defined using a light-use efficiency approach:

$$fCO2_{gc}^{av}[light] = \epsilon lue \cdot F_{leaf} \cdot f\Gamma^{av} \tag{30}$$

where $\epsilon lue$ is a globally uniform factor accounting for light-use efficiency, $F_{leaf}$ is the fraction of the surface covered by leaves and $f\Gamma^{av}$ is the amount of short-wave solar radiation. The water-limited gross primary productivity is described using a water-use efficiency approach:

$$fCO2_{gc}^{av}[water] = \epsilon wue \cdot \frac{x\mu CO2_g^a - x\mu CO2_l^v}{x\mu H2O_l^v - x\mu H2O_g^a} \cdot fH2O_g^{va} \tag{31}$$

where $\epsilon wue$ is a factor that accounts for water-use efficiency and also includes the lower diffusion of $CO_2$ with respect to water vapour, $x\mu H2O_l^v - x\mu H2O_g^a$ is the gradient between plant water potential and atmospheric water vapour potential. $x\mu H2O_l^v$ is described as a linear function of plant water content (Roderick and Canny, 2005; Schymanski, 2007):

$$x\mu H2O_l^v = pwiltH2O_l^s \cdot \left( \frac{rH2O_l^v}{pmaxH2O_l^v} - max\left(1.0, \frac{rH2O_l^v}{pmaxH2O_l^v}\right)\right) \cdot cGrav \tag{32}$$

where $pwiltH2O_l^s$ is the permanent wilting point, $cGrav$ is the gravitational acceleration and $\frac{rH2O_l^v}{pmaxH2O_l^v}$ is the relative plant water content. $x\mu H2O_g^a$ is calculated according to Kleidon and Schymanski (2008). $x\mu CO2_g^a - x\mu CO2_l^v$ is the gradient in the chemical potential of $CO_2$ across the leaf-air interface. Both $x\mu CO2_g^a$ and $x\mu CO2_l^v$ are derived as functions of pressure, temperature and tabulated values of the energy of formation (Engel and Reid, 2006). $CO_2$ inside the leaf is assumed to be 70% of the atmospheric $CO_2$ (Wong et al., 1979).

Respiration, which accounts for plant growth costs and maintenance is calculated in each time step as 50% of the GPP (Ryan, 1991). From the respired carbon half goes to the soil ($fCO2_{cg}^{vs}$) and half goes to the atmosphere ($fCO2_{cg}^{va}$). Therefore the net pri-

mary productivity NPP is calculated as the difference between GPP and respiration:

$$fC_{co}^{v} = fCO2_{gc}^{av} - (fCO2_{cg}^{va} + fCO2_{cg}^{vs}) \quad (33)$$

Litter fall $fC_{o}^{vs}$ is calculated using a residence time $p\tau C_{o}^{v}$ of structural biomass in the soil:

$$fC_{o}^{vs} = \frac{rC_{o}^{v}}{p\tau C_{o}^{v}} \quad (34)$$

### 2.6.2. Water fluxes

Transpiration is calculated as the minimum between the water stored in the vegetation and the atmospheric demand.

$$fH2O_{g}^{va} = \min\left(fpotH2O_{g}^{sa}, \frac{rH2O_{l}^{v}}{pdt} + fH2O_{l}^{sv}\right) \quad (35)$$

where the atmospheric demand $fpotH2O_{g}^{sa}$ is calculated according to Equation 7. As with bare soil evaporation, the phase transition from liquid to gaseous water inside the leaf is not explicitly modelled here. Root water uptake $fH2O_{l}^{sv}$ is calculated in JESSY-WATER (Equation 8).

### 2.6.3. Balance equations

The pool of sugars and starch in the vegetation $rC_{c}^{v}$ and the structural biomass $rC_{o}^{v}$ are the result from the balance between carbon uptake, respiration and litter fall.

$$\frac{d}{dt}dC_{c}^{v} = fCO2_{gc}^{av} - fCO2_{cg}^{va} - fCO2_{cg}^{vs} - fC_{co}^{v} \quad (36)$$

$$\frac{d}{dt}dC_{o}^{v} = fC_{co}^{v} - fC_{o}^{vs} \quad (37)$$

From the total vegetation biomass the proportion of green biomass, or vegetative cover, is estimated from an empirical parametrisation:

$$Cover = \left(\arctan\left(\frac{pa^{v} \cdot rC_{o}^{v} - pb^{v}}{pc^{v}}\right)/pd^{v} + pe^{v}\right) \cdot pf^{v} \quad (38)$$

where the parameters $pa^{v}$ to $pf^{v}$ are set to values which result in a realistic distribution of forested area with respect to the borders of the Taiga and Savannah biomes. The vegetative cover is limited to values between 0 and 1.

The amount of water in vegetation is limited to be positive and is determined by the balance between water uptake and evapotranspiration:

$$\frac{d}{dt}rH2O_{l}^{v} = fH2O_{l}^{sv} - fH2O_{l}^{va} \quad (39)$$

## 3. Model setup

### 3.1. Climate input data

To evaluate JESSY and SIMBA for present-day conditions, they are run with climate data from the NASA Land Surface and Hydrology archive from the years 1971 to 2006 (Sheffield et al., 2006). This data includes daily values of short-wave radiation, downwelling long-wave radiation, precipitation, daily average air temperature and daily minimum air temperature. The temperature data is measured at 2 m height and it is assumed that it is ap-

proximately equal to the surface temperature $xT^{as}$ in the model. Since the model needs terrestrial long-wave radiation, the upwelling long-wave radiation is subtracted from the downwelling one. Upwelling long-wave radiation is derived from the surface temperature according to the Stefan-Boltzmann-law and is then multiplied by an emissivity of 0.97. The model needs also relative humidity as input data. Hence, the saturation vapour pressure is calculated according to the equation psat $= 0.6108e^{17.27\frac{T-273}{T-35.7}}$ where T is the daily mean temperature in degrees Kelvin (Allen et al., 1998). The same is done for the minimum daily temperature assuming that the actual vapour pressure is equal to psat($T_{\min}$). Relative humidity then results from RH = psat($T_{\min}$)/psat($T$).

It has to be mentioned that feedbacks with the climate forcing are not simulated in this study for reasons of computational speed. It is, however, possible to couple JESSY and SIMBA to an atmospheric model.

## 3.2. Setup of the simulations

The model is run on a global rectangular grid with a resolution of 2.8125 degrees (T42 resolution). The length of one simulation is 470 years, such that all variables, particularly the thickness of the ice sheets in the polar regions and the amount of soil carbon have reached a steady state in the model. To control the assumption of steady state, a 2070-year model run is used. The model outputs of the two runs differ by around 5 percent.

All model output variables are derived by averaging over the last 10 years of the simulation. Averaging over longer periods, e.g. 30 years, does not change the model output much, the difference between the values is less than 5 percent. If the averaging period is shorter, however, some output variables of the model change, which is not surprising. The Budyko-curve, for instance, is based on the assumption of zero change in soil water storage, which is only valid for longer periods of time.

## 3.3. Datasets used for model evaluation

To evaluate JESSY and SIMBA, the model output is compared to a number of datasets. These datasets contain in our view the most important variables to characterise the water and carbon budgets at the land surface: Runoff, evapotranspiration, Net Primary Productivity (NPP), and soil carbon.

### 3.3.1. Runoff

Runoff output from JESSY is compared to river basin discharge data from the 35 largest catchments by area of the world. To identify the grid cells of the model contributing to a certain basin, the mask from Vorosmarty et al. (2000) is used. The discharge data is taken from Dai and Trenberth (2002). This dataset contains 200 river basins sorted by discharge volume. Consequently, some basins which

have a large area but show no or only little amounts of runoff are not included. The runoff values for these basins are derived from additional literature (Probst and Tardy, 1987; Shahin, 1989; Aladin et al., 2005; Meshcherskaya and Golod, 2003). Since the dataset does not allow for a distinction between surface runoff and baseflow, the sum of the model output variables $fH2O_l^{ac}$ and $fH2O_l^{sc}$ (see Section 2.4) is compared to the river basin discharge data.

#### 3.3.2. Evapotranspiration

Complete global datasets of directly measured evapotranspiration are, to our knowledge, not available. We therefore use an indirect method to evaluate JESSY and SIMBA in this respect, based on the Budyko-curve (Budyko, 1974) which is confirmed by a large amount of empirical data (Budyko, 1951, 1961; Donohue et al., 2007). The Budyko-curve predicts evapotranspiration as a function of a climate index, which only depends on net radiation and precipitation. These two variables are both provided by the climate dataset used as model input. The agreement between model output and the Budyko-curve is estimated by calculating the climate index for each of the 35 largest river basins as a function of the mean net radiation and precipitation over the basin. The predicted evapotranspiration is then compared to the mean modelled evapotranspiration over the basin.

#### 3.3.3. Net Primary Productivity and Soil carbon

A global estimate of Net Primary Productivity (NPP) is provided by Cramer et al. (1999). This estimate results from the mean of the predictions of NPP of 17 different vegetation models. It consequently allows for drawing a comparison between SIMBA and other global vegetation models. Soil carbon data for the first meter of the soil column is taken from IGBP-DIS (1998). For both NPP and soil carbon latitudinal profiles of model output and data are compared.

## 4. Model evaluation

### 4.1. Model output

JESSY and SIMBA allow for the quantification of several biogeochemical reservoirs and fluxes such as soil moisture, soil carbon, runoff, evapotranspiration and NPP. As an example, two of these variables are shown in Figure 2.

### 4.2. Sensitivity analysis

The output variables used for the sensitivity analysis of JESSY and SIMBA are the latitudinal pattern of Net Primary Productivity (NPP) and the ratio of runoff to evapotranspiration, expressed by the Budyko-curve (Budyko, 1974). These two quantities largely determine the patterns and values of the other variables used for the evaluation of the model: Runoff, evapotranspiration and soil carbon. The model

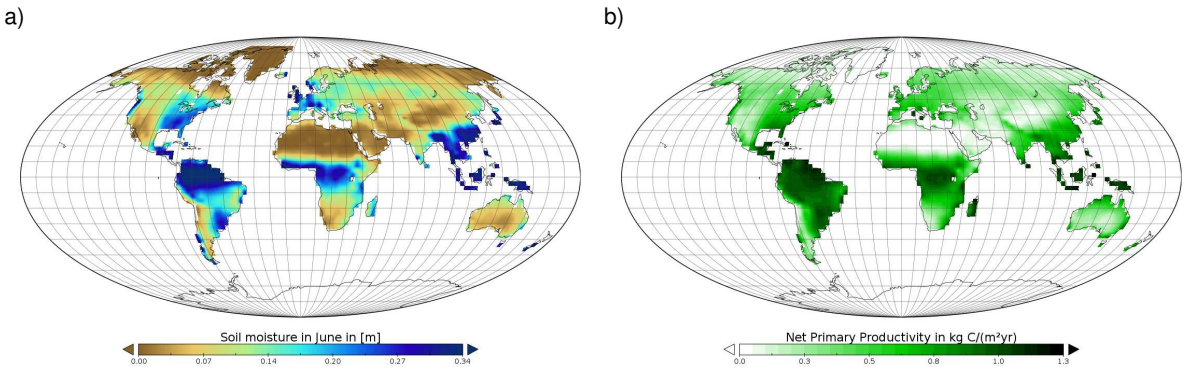


**Figure 2:** Global distribution of a) soil moisture and b) NPP, the values are averages over the last 10 years of a simulation.

sensitivity is tested with respect to all parameters that have unknown values. These include soil depth, soil type, conductivity at the soil-root-interface, time scale of baseflow , parameters controlling water-use efficiency and light-use efficiency, and the soil carbon turnover time scale (see Table 3).

The model is most sensitive to the conductivity at the soil-root-interface, which controls transpiration by vegetation and which subsequently strongly influences the partitioning between evapotranspiration and runoff. It also affects the latitudinal pattern of NPP, which can be explained by the fact that NPP becomes limited by evapotranspiration in case of declining root water uptake.

The parameters controlling water-use efficiency and light-use efficiency, $\epsilon wue$ and $\epsilon lue$, have a strong effect on the total value of NPP, which can be easily seen from Equations (30) and (31). Furthermore, the proportion of $\epsilon wue$ to $\epsilon lue$ determines where vegetation is water limited and where it is light limited.

The value of the conductivity at the interface between soil and river channel controls the ratio of surface runoff to baseflow. Low values of this parameter lead to slightly enhanced evapotranspiration, since baseflow is reduced and therefore plants can transpire more water. This has a positive influence on NPP.

The soil type is characterised by two parameters (van Genuchten, 1980; Mualem, 1976) which determine soil water storage capacity. The influence of these parameters on runoff, however, is small and the bucket is not sensitive to soil type.

Changing soil depth $p\Delta Z^s$ affects the water storage capacity of the bucket. Consequently, the ratio of surface runoff to baseflow is shifted towards surface runoff with decreasing soil depth. Also total runoff increases slightly, since the water that is available for the vegetation is reduced at shallow soil depths. This also leads to a slight reduction of NPP with decreasing soil

depth.

While the latitudinal pattern of soil carbon is strongly influenced by NPP, its total amount depends also on the time scale of soil carbon turnover, $p\tau C_o^s$.

In summary, the conductivity at the soil root interface has the strongest effect on the model output, since it controls both evapotranspiration and NPP. Varying soil properties and the parameters controlling water-use efficiency and light-use efficiency, however, only leads to small changes in the model output. Thus, given the data used to evaluate the model, more than one parametrisation of the model leads to good predictions of the data. The parameter values shown in Table 3 are one example of a model parametrisation that generates a realistic model output with respect to the Budyko-curve and the latitudinal pattern of NPP, considering the datasets from Section (3).

### 4.3. Comparing the model with observational data

The results of the comparison between model output and data are presented in Figure 3. It can be seen that the general patterns of runoff, evapotranspiration, NPP and soil carbon simulated by the model correspond well with the available empirical observations. Also the absolute values agree relatively well with the ones from the evaluation data sets. However, modelled runoff in the northern temperate regions seems to be slightly too high according to the Budyko-curve. Furthermore, modelled runoff in arid catchments seems to be higher than the observed one. A possible reason for these results is given in the discussion.

## 5. Discussion

Although model output and evaluation data show good agreement in general, some aspects of the climate input data and the datasets used for evaluating the model need further discussion.

A thorough analysis of the quality of the input data lies beyond the scope of this study. Nevertheless, the consistency of the river basin discharge dataset and the LSH climate data is checked using the Budyko-curve (see Section 3). The climate data based runoff from each of the 35 largest river basins can be derived by subtracting the evapotranspiration predicted by the Budyko-curve from the mean precipitation over the respective basin. This is then compared to the river basin discharge data. The agreement between climate data based runoff and measured one is reasonable (see Figure 4).

In general, runoff derived by the Budyko-curve seems to be smaller than the measured one, especially for regions in high latitudes and some arid regions (Figure 3). These regions exhibit large-scale flooding events which prevent the vegetation from taking up the available water. Consequently, the Budyko-curve probably overestimates the amount of water available for evapotanspiration since it is based on annual mean values of precipitation and

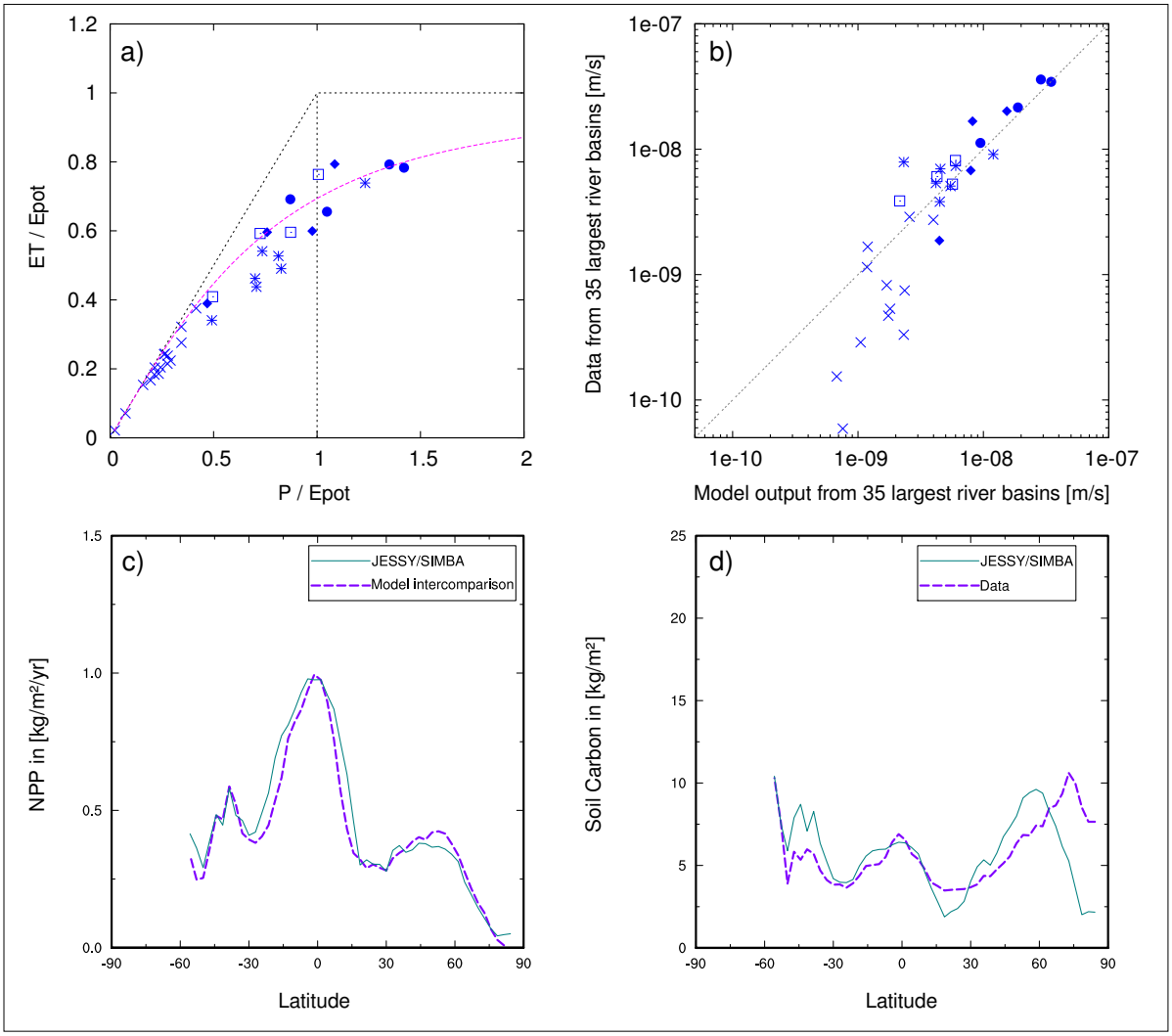


**Figure 3:** a) Modelled evapotranspiration averaged over a basin plotted against the theoretical Budyko-curve (magenta, dashed) for the 35 world's largest river basins. b) scatterplot of modelled runoff and observed runoff for the 35 largest river basins of the world (Dai and Trenberth, 2002). • corresponds to humid tropical, ⧫ humid subtropical, ⊡ temperate, ⁕ cold continental and × (semi) arid climate regions. c) latitudinal pattern of modelled NPP (blue, solid) and the mean NPP of 17 global vegetation models (magenta, dashed). d) latitudinal pattern of modelled (blue, solid) and measured (magenta, dashed) soil carbon, both accumulated over the first meter of the soil. All model estimates are average values over the last 10 years of a simulation .

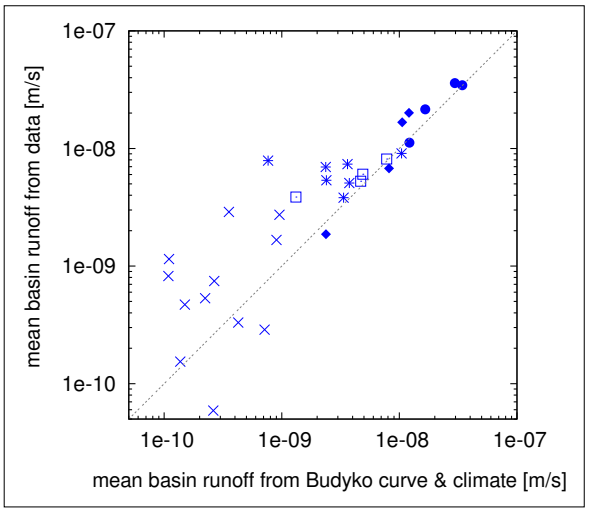


**Figure 4:** scatterplot of measured runoff and runoff derived by combining the Budyko-curve and climate input data for the 35 largest river basins of the world. • corresponds to humid tropical, ♦ to humid subtropical, ⊡ to temperate, ✳ to cold continental and × to (semi) arid climate regions.

radiation. A temporal separation of water supply and demand is not explicitly considered in Budyko's framework (Koster and Suarez, 1999). Assuming that the river basin discharge data is not biased, another explanation for the difference between runoff data and predictions by the Budyko-curve could be a general underestimation of precipitation in the climate data in northern temperate regions, which is not unrealistic (Milly and Dunne, 2002). Hence, the small overestimation of runoff by the bucket models used in JESSY with respect to the Budyko-curve can be explained by the possible underestimation of runoff by the Budyko-curve in certain regions of the world.

Comparing the model output with runoff data from the 35 world's largest catchments, runoff seems to be overestimated in arid regions (Figure 3). Assuming the climate data in these regions to be correct, a possible explanation for this result is the extraction of water by agriculture in most of the respective catchments, which is not accounted for in the model and demonstrably leads to a strong decrease in runoff. The slight underestimation of runoff by the model in northern temperate regions might result from underestimation of precipitation in the climate data in this region as mentioned above.

## 6. Summary and conclusions

The JESSY/SIMBA model allows for a simple and fast modelling of land surface processes at the global scale. Global biogeochemical fluxes such as evapotranspiration, runoff and NPP and reservoirs such as soil moisture or soil carbon can be quantified. In spite of its simplicity, the JESSY/SIMBA model is able to reproduce a variety of global observational datasets with reasonable accuracy. This is important, since it shows that earth system models do not have to be complex to produce good results. Increasing model complexity usually leads to a higher number of unknown model parameters which have to be determined by calibrating the model against empirical datasets. By doing so, however, it is implicitly assumed that differences between model output and data are due to the unknown parameter values

and the remainder of the model is correct. This is a very general problem faced by almost every model used in earth system analysis. The number of unknown parameters should consequently be reduced to a minimum. The model presented here could be used as a basis for a more parsimonious approach to biogeochemical modelling.

## 7. Acknowledgements

The authors want to thank Ryan Pavlick, Björn Reu and Nate Brunsell for their helpful support. This study has been financially supported by the Helmholtz Alliance for Planetary Evolution and Life.

## References

Aladin, N., Cretaux, J.-F., Plotnikov, I. S., Kouraev, A. V., Smurov, A. O., Cazenave, A., Egorov, A. N., and Papa, F.: Modern hydro-biological state of the Small Aral sea, Environmetrics, 16, 375–392, 2005.

Allen, R. G., Pereira, L. S., Raes, D., and Smith, M.: Crop evapotranspiration - Guidelines for computing crop water requirements, FAO - Food and Agriculture Organization of the United Nations, Rome, Italy, 56, 1998.

Arens, S. and Kleidon, A.: Global sensitivity of weathering rates to atmospheric CO2 under the assumption of saturated river discharge, Mineralogical Magazine, 72, 305–308, 2008.

Blackburn, E., Liang, X., and Wood, E. F.: The Effect of Soil Thermal Conductivity Parameterization on Surface Energy Fluxes and Temperatures, J. Atmos. Sci., 55, 1209–1224, 1997.

Budyko, M., ed.: Climate and life, Academic Press, New York, 1974.

Budyko, M. I.: On the Influence of Reclamation Practices on Potential Evaporation, Bull. Acad. Sci. USSR, Ser.: Geogr., 1, 16–35, 1951.

Budyko, M. I.: On the Thermal Zonation of the Earth, Meteorol. Gidrol., 6, 144–151, 1961.

Carsel, R. F. and Parrish, R. S.: Developing Joint Probability Distributions of Soil Water Retention Characteristics, Water Resour. Res., 24, 755–769, 1988.

Cramer, W., Kicklighter, D. W., Bondeau, A., Moore III, B., Churkina, G., Nemry, B., Ruimy, A., and Schloss, A.: Comparing global models of terrestrial Net Primary Productivity (NPP): overview and key results, Global Change Biology, 5, 1–15, 1999.

Dai, A. and Trenberth, K. E.: Estimates of Freshwater Discharge from Continents: Latitudinal and Seasonal Variations, J. Hydrometeor., 3, 660–687, 2002.

Dewar, R.: A simple model of light and water use efficiency for Pinus radiata, Tree Physiol., 17, 259–265, 1997.

Donohue, R. J., Roderick, M. L., and McVicar, T. R.: On the importance of including vegetation dynamics in Budykos hydrological model, Hydrol. Earth Syst. Sci., 11, 983–995, 2007.

Engel, T. and Reid, P.: Physikalische Chemie, Pearson Studium, 2006.

Fang, C. and Moncrieff, J.: A model for soil $CO_2$ production and transport 1: Model development, Agricultural and Forest Meteorology, 95, 225–236, 1999.

Hillel, D., ed.: Environmental Soil Physics, Academic Press, 1998.

IGBP-DIS: SoilData(V.0) A program for creating global soil-property databases, IGBP Global Soils Data Task, France, 1998.

Kleidon, A.: Beyond Gaia: thermodynamics of life and earth system functioning, Climate Change, 66, 271–319, 2004.

Kleidon, A.: The climate sensitivity to human appropriation of vegetation productivity and its thermodynamic characterization, Glob Planet Change, 54, 109–127, 2006.

Kleidon, A. and Schymanski, S.: Thermodynamics and optimality of the water budget on land: A review, Geophys. Res. Lett., 35, 2008.

Knorr, W. and Heimann, M.: Impact of drought stress and other factors on seasonal land biosphere CO2 exchange studied through an atmospheric tracer transport model, Tellus B, 47, 471–489, 1995.

Koster, R. J. and Suarez, M. J.: A Simple Framework for Examining the Interannual Variability of Land Surface Moisture Fluxes, J. Climate, 12, 1911–1917, 1999.

Lunkeit, F., Fraedrich, K., Jansen, H., Kirk, E., Kleidon, A., and Luksch, U.: Planet simulator reference manual, 2004.

McNaughton, K. G. and Jarvis, P. G.: Predicting effects of vegetation changes on transpiration and evaporation, in: Water Deficits and Plant Growth, edited by Kozlowski, T. L., vol. 7, pp. 1–47, Academic Press, New York, 1983.

Meshcherskaya, A. V. and Golod, M. P.: Statistical Estimates of the Dependence of the Caspian Sea Level and the Volga Runoff on the Amount of Precipitation onto the Volga Watershed, Water Resources, 30, 23–33, 2003.

Milly, P. C. D. and Dunne, K. A.: Macroscale water fluxes: 2. Water and energy supply control of their interannual variability, Water Resour. Res., 38, 1206, 2002.

Monteith, J. L., Huda, A. K. S., and Midya, D.: RESCAP: a resource capture model for sorghum and pearl millet, in: Modelling the growth and development of sorghum and pearl millet, edited by SM, V., HLS, T., and G, A., vol. 12, pp. 30–38, 1989.

Mualem, Y.: A new model for predicting the hydraulic conductivity of unsaturated porous media, Water Resour. Res., 12, 513–522, 1976.

Probst, J. L. and Tardy, Y.: Long Range Streamflow and World Continental Runoff Fluctuations since the Beginning of this Century, J.Hydrol., 94, 289–311, 1987.

Roderick, M. L. and Canny, M. J.: A mechanical interpretation of pressure chamber measurements - what does the strength of the squeeze tell us?, Plant Physiology and Biochemistry, 43, 323–336, 2005.

Ryan, M. G.: Effects of Climate Change on Plant Respiration, Ecological Applications, 1, 157–167, 1991.

Schymanski, S. J.: Transpiration as the Leak in the Carbon Factory: A Model of Self-Optimising Vegetation, Ph.D. thesis, The University of Western Australia, 2007.

Shahin, M.: Review and Assessment of Water Resources in the Arab Region, Water International, 14, 206–219, 1989.

Sheffield, J., Goteti, G., and Wood, E. F.: Development of a 50-yr high-resolution global dataset of meteorological forcings for land surface modeling, J. Climate, 19, 3088–3111, 2006.

van Genuchten, M. T.: A closed-form equation for predicting the hydraulic conductivity of unsaturated soils, Soil Sci. Soc. Am. J., 44, 892–898, 1980.

Vorosmarty, C., Fekete, B., Meybeck, M., and Lammers, R.: Geomorphometric attributes of the global system of rivers at 30-minute spatial resolution, Journal of Hydrology, 237, 17–39, 2000.

Wong, S. C., Cowan, I. R., and Farquhar, G. D.: Stomatal conductance correlates with photosynthetic capacity, Nature, 282, 424–426, 1979.

## A. Variables and parameters used in the model

**Table 2:** Description of variables

| | Symbol | Description | Units |
|---|---|---|---|
| pools | $rH2O_l^v$ | water in vegetation | m |
| | $rH2O_l^s$ | soil water | m |
| | $rH2O_s^s$ | frozen soil water | m |
| | $rH2O_s^{as}$ | snow pack | m |
| | $rC_o^v$ | structural biomass of vegetation | kg C $m^{-2}$ |
| | $rC_c^v$ | sugars & starch in vegetation | kg C $m^{-2}$ |
| | $rC_o^s$ | soil organic matter | kg C $m^{-2}$ |
| | $rCO2^s$ | total $CO_2$ in soil | moles $m^{-2}$ |
| | $rCO2_d^s$ | $CO_2$ dissolved in soil water | moles $m^{-2}$ |
| | $rCO2_g^s$ | $CO_2$ in soil air | moles $m^{-2}$ |
| fluxes | $fH2O_l^{as}$ | precipitation | m $s^{-1}$ |
| | $fH2O_l^{sv}$ | root water uptake | m $s^{-1}$ |
| | $fH2O_g^{va}$ | transpiration | m $s^{-1}$ |
| | $fH2O_g^{sa}$ | evaporation | m $s^{-1}$ |
| | $fH2O_l^{ac}$ | surface runoff | m $s^{-1}$ |
| | $fH2O_l^{sc}$ | baseflow | m $s^{-1}$ |
| | $fH2O_{sl}^{as}$ | snow melt | m $s^{-1}$ |
| | $fCO2_{gc}^{av}$ | vegetation gross carbon uptake GPP | kg C $m^{-2}s^{-1}$ |
| | $fCO2_{co}^{v}$ | vegetation net carbon uptake NPP | kg C $m^{-2}s^{-1}$ |
| | $fCO2_{cg}^{va}$ | leaf respiration | kg C $m^{-2}s^{-1}$ |
| | $fCO2_{cg}^{vs}$ | root respiration | kg C $m^{-2}s^{-1}$ |
| | $fC_o^{vs}$ | Litter production | kg C $m^{-2}s^{-1}$ |
| | $fCO2_{og}^{ss}$ | soil respiration | kg C $m^{-2}s^{-1}$ |
| | $fCO2_d^{as}$ | input of $CO_2$ though rain | moles $m^{-2}s^{-1}$ |
| | $fCO2_g^{sa}$ | soil $CO_2$ efflux | moles $m^{-2}s^{-1}$ |
| | $fQ^{as}$ | heat flux into the soil | W $m^{-2}$ |
| | $fQ_i^s$ | heat flux from soil column i into column i+1 | W $m^{-2}$ |
| states | $xT^{s,i}$ | soil temperature in the ith layer | K |
| | $xT^{as}$ | surface temperature | K |
| | $xKQ^{s,i}$ | soil heat conductivity in the ith layer | W $m^{-1}K^{-1}$ |
| | $x\mu H2O_g^a$ | water vapour potential | $m^2$ $s^{-2}$ |
| | $x\mu H2O_l^v$ | vegetation water potential | $m^2$ $s^{-2}$ |

**Table 3:** Description of model parameters. Parameters with the reference ⁕ are set by personal assessment while parameters marked by ⊙ are calibrated to values which lead to reasonable model output considering the data used to evaluate the model.

| Parameter | Description | Value | Units | Reference |
|---|---|---|---|---|
| $cQH2O_{lg}$ | latent heat of vaporization | 2.45E6 | J $kg^{-1}$ | |
| $c\rho H2O_l$ | density of liquid water | 1000.0 | kg $m^{-3}$ | |
| $c\gamma$ | psychometric constant | 65.0 | Pa $K^{-1}$ | |
| $cTH2O_{sl}$ | melting temperature | 273.15 | K | |
| $ccpH2O_s$ | heat capacity of ice | 2.05E6 | J $m^{-3}K^{-1}$ | |
| $ccpH2O_l$ | heat capacity of water | 4.18E6 | J $m^{-3}K^{-1}$ | |
| $psa1$ | parameter to calculate vapour pressure | 17.269 | | (Allen et al., 1998) |
| $psa2$ | parameter to calculate vapour pressure | 237.3 | K | (Allen et al., 1998) |
| $psa3$ | parameter to calculate vapour pressure | 610.8 | Pa | (Allen et al., 1998) |
| $p\tau H2O_s^{as}$ | snow loss time scale | 3.0e-10 | $s^{-1}$ | ⁕ |
| $pKH2O_l^{sv}$ | soil-root conductivity | 5.5E-08 | m $s^{-1}$ | ⊙ |
| $p\tau H2O_l^s$ | timescale of baseflow | 3.0e+7 | s | ⊙ |
| $p\Delta Z^s$ | soil depth | 1.0 | m | ⊙ |
| $pmaxH2O_l^s$ | relative soil water content at saturation | 0.345 | m | $p\Delta Z^s \cdot (p\Theta s^s - p\Theta r^s)$ |
| $p\Theta r^s$ | residual relative soil water content | 0.065 (sandy loam)<br>0.068 (clay)<br>0.045 (sand) | | (Carsel and Parrish, 1988) |
| $p\Theta s^s$ | maximum relative soil water content | 0.41 (sandy loam)<br>0.38 (clay)<br>0.43 (sand) | | (Carsel and Parrish, 1988) |
| $\epsilon lue$ | factor for light-use efficiency | 120 | | ⊙ |
| $\epsilon wue$ | factor for water-use efficiency | 3.5e-10 | | ⊙ |
| $pwiltH2O_l^s$ | permanent wilting point | 150.0 | m | (Hillel, 1998) |
| $pmaxH2O_l^v$ | relative plant water content at saturation | 1.0 | m | ⁕ |
| $p\tau C_o^v$ | carbon residence time in vegetation | 3.1e+8 | s | ⁕ |
| $p\tau C_o^s$ | soil carbon turnover time scale | 1.2e+9 | s | ⊙ |
| $pq10ss$ | Q10 value of litter decomposition | 2.0 | | (Knorr and Heimann, 1995) |